AFR Engineering
Academy

Heat and Mass Transfer of a Co₂ Binary Mixture: An Analytical Approach

[1]Olayiwola, R. O., [2]Cole, A. T., [3]Shehu, M. D., [4]Oguntolu, F. A.
[1, 2, 3, 4] Department of Mathematics,
Federal University of Technology, Minna, Nigeria

Corresponding Email: olayiwola.rasaq@futminna.edu.ng

Keywords: carbon dioxide, critical point, polynomial approximation method, solvent, supercritical fluid.

In this paper, an analytical solution for describing heat and mass transfer between a droplet of organic solvent and a compressed antisolvent taking into consideration the viscous energy dissipation and heat and mass transfer between the surface and the droplet by convection is presented. We assume that the solvent and the antisolvent are fully miscible and have the same temperature. We also assume both the initial temperature of the mixture and the initial carbon dioxide concentration depends on the space variable. The governing equations formulated based on the conservation of total mass, chemical species, momentum and energy were solved analytically using polynomial approximation method. The results obtained are presented graphically and discussed. The results revealed the effects of operating parameters on droplet lifetime. This results might be used for interpretation or experiments planning of the more complex real supercritical antisolvent process.

HEAT AND MASS TRANSFER OF A CO_2 BINARY MIXTURE: AN ANALYTICAL APPROACH

Olayiwola, R. O.; Cole, A. T.; Shehu, M. D.; Oguntolu, F. A.

Department of Mathematics,

Federal University of Technology, Minna, Nigeria.

E-mail.: olayiwola.rasaq@futminna.edu.ng

Abstract

In this paper, an analytical solution for describing heat and mass transfer between a droplet of organic solvent and a compressed antisolvent taking into consideration the viscous energy dissipation and heat and mass transfer between the surface and the droplet by convection is presented. We assume that the solvent and the antisolvent are fully miscible and have the same temperature. We also assume both the initial temperature of the mixture and the initial carbon dioxide concentration depends on the space variable. The governing equations formulated based on the conservation of total mass, chemical species, momentum and energy were solved analytically using polynomial approximation method. The results obtained are presented graphically and discussed. The results revealed the effects of operating parameters on droplet lifetime. This results might be used for interpretation or experiments planning of the more complex real supercritical antisolvent process.

***Keywords and phrases*:** carbon dioxide, critical point, polynomial approximation method, solvent, supercritical fluid.

1. Introduction

A supercritical fluid is a substance that is at a temperature and pressure above its critical point, where distinct liquid and gas phases do not exist. It can diffuse through solids like a gas, and dissolve materials like a liquid (Padrela *et al.*, 2009).

Supercritical fluids have different properties compared to regular fluids and could play a role as life-sustaining solvents on other worlds. Even on Earth, some bacterial species have been shown to be tolerant to supercritical fluids (Budisa and Schulze-Makuch, 2014).

Supercritical fluids are very important in the modern chemical technologies and have a very good potential to be used in various fields. One of the main advantages of supercritical fluids is that they are classified under green technology and are hence environmentally friendly. They are majorly used in the chemical industries for extraction purposes as they give excellent results due to their unique properties. Other prominent applications are in the pharmaceutical industry for micro ionisation and for analytical samples in chromatography as well as dry cleaning, drying and impregnation. Most commonly used supercritical fluid is carbon dioxide which is popularly used in Decaffeination (Yash, 2015).

Carbon dioxide: CO2 is a very attractive supercritical fluid for many reasons:

* Very cheap and abundant in pure form (food grade) worldwide;

* Nonflammable and not toxic;

* Environment-friendly, as non-polluting gas and as most of CO2 is manufactured from waste streams (mainly fertilizer plants gaseous effluents).

Now we consider a 'pseudo' droplet of solvent (hydrocarbon droplet) immersed in a compressed antisolvent (carbon dioxide) in miscible conditions. The space variable (droplet radius) is r, $0 \le r \le R$, and time is t, $t > 0$. The state variables depending on (r,t) are mixture temperature T, carbon dioxide mole fraction X_c, solvent mole fraction X_h, velocity of droplet u and pressure p. A similar problem but with negligible viscous energy dissipation, convective flux and heat and mass transfer was considered in Kumar *et al*. (2012), Chong *et al*. (2009), Wu *et al*. (2012) and Almeida *et al*. (2015).

In this paper, the aim is to establish an approximate analytical solution capable of predicting the composition of hydrocarbon and carbon dioxide in EOR process. For this we shall follow the method proposed in [illegible] and [illegible] (20[illegible]).

2. Model Formulation

In formulating our model, the following assumptions were considered:

(i) The solvent and the antisolvent are fully miscible so only one equation is needed to describe the mass transfer.

(ii) The medium is not stagnant so the convective flux can be considered.

(iii) The radial velocity (velocity of droplet) is non-zero because of temperature change and mixing of carbon dioxide and hydrocarbons.

(iv) The heat and mass transfer between the surface and the mixture take place by convection.

(v) The spherical symmetry is considered, making the problem one-dimensional.

(vi) The viscous energy dissipation is considered.

(vii) There is no heat source.

The diffusive flux is assumed to be proportional to the concentration gradient as described by Fick's law:

$$N_c = -\rho D \nabla X_c + X_c N \qquad (1)$$

The mass balance on carbon dioxide reads:

$$\frac{\partial}{\partial t}(\rho X_c) + \nabla \cdot (-\rho D \nabla X_c + X_c N) = 0 \qquad (2)$$

The continuity equation required to find the convective flux N is

$$\frac{\partial \rho}{\partial t} + \nabla \cdot N = 0 \tag{3}$$

Multiplying (3) by Y_i and combining with (2) yields:

$$\rho \frac{\partial Y_i}{\partial t} + N\nabla \cdot Y_i = \nabla \cdot \left(\rho D \nabla Y_i\right) \tag{4}$$

In a similar manner, momentum and energy conservation equations can be obtained as:

$$\rho \frac{\partial u}{\partial t} + N\nabla \cdot u = -\frac{\partial p}{\partial x} + \frac{\partial}{\partial x}\left(2\mu \frac{\partial u}{\partial x} - \frac{2}{3}\mu \nabla \cdot u\right) \tag{5}$$

$$c_p\left(\rho \frac{\partial T}{\partial t} + N\nabla \cdot T\right) = \nabla \cdot \left(\lambda \nabla T\right) + \rho c_p D \frac{1000}{M}\frac{\partial Y_i}{\partial x}\frac{\partial T}{\partial x} + \mu\left(2\left(\frac{\partial u}{\partial x}\right)^2 - \frac{2}{3}\left(\frac{\partial u}{\partial x}\right)^2\right) \tag{6}$$

Introducing an apparent flux to replace convective flux (i.e., $N = \rho u$) yields in one-dimensional Cartesian coordinates:

$$\frac{\partial \rho}{\partial t} + \frac{\partial}{\partial x}\left(\rho u\right) = 0 \tag{7}$$

$$\rho\left(\frac{\partial u}{\partial t} + u\frac{\partial u}{\partial x}\right) = -\frac{\partial p}{\partial x} + \frac{\partial}{\partial x}\left(2\mu \frac{\partial u}{\partial x} - \frac{2}{3}\mu \frac{\partial u}{\partial x}\right) \tag{8}$$

$$\rho\left(\frac{\partial Y_i}{\partial t} + u\frac{\partial Y_i}{\partial x}\right) = \frac{\partial}{\partial x}\left(\rho D \frac{\partial Y_i}{\partial x}\right) \tag{9}$$

$$\rho c_p\left(\frac{\partial T}{\partial t} + u\frac{\partial T}{\partial x}\right) = \frac{\partial}{\partial x}\left(\lambda \frac{\partial T}{\partial x}\right) + \rho c_p D \frac{1000}{M}\frac{\partial Y_i}{\partial x}\frac{\partial T}{\partial x} + \mu\left(2\left(\frac{\partial u}{\partial x}\right)^2 - \frac{2}{3}\left(\frac{\partial u}{\partial x}\right)^2\right) \tag{10}$$

We can eliminate the continuity equation (7) by means of streamline function (see, Olayiwola (2015)).

$$\eta(x,t)=\left(\rho^{2}\right)^{\frac{1}{2}}\int_{0}^{x}\rho(x,t)dx$$

(11)

The coordinate transformation becomes,

$$\frac{\partial}{\partial x}\rightarrow\frac{\partial}{\partial\eta}\frac{\partial\eta}{\partial x}=\frac{\partial}{\partial\eta}$$

(12)

$$\frac{\partial}{\partial t}\rightarrow\frac{\partial}{\partial\eta}\frac{\partial\eta}{\partial t}+\frac{\partial}{\partial t}=-u\frac{\partial}{\partial\eta}+\frac{\partial}{\partial t}$$

(13)

We make the additional assumptions that c_p, λ, μ and ρD are constant. Although these assumptions could be relaxed in the future, they considerably simplify the equations. The equations can be simplified as

$$\frac{\partial u}{\partial t}=-\frac{1}{\rho}\frac{\partial p}{\partial\eta}+\upsilon\frac{\partial}{\partial\eta}\left(2\frac{\partial u}{\partial\eta}-\frac{2}{3}\frac{\partial u}{\partial\eta}\right)\tag{14}$$

$$\frac{\partial X_s}{\partial t}=D\frac{\partial}{\partial\eta}\left(\frac{\partial X_s}{\partial\eta}\right)\tag{15}$$

$$\frac{\partial T}{\partial t}=\frac{\lambda}{\rho c_p}\frac{\partial}{\partial\eta}\left(\frac{\partial T}{\partial\eta}\right)+\frac{1000D}{M}\frac{\partial X_s}{\partial\eta}\frac{\partial T}{\partial\eta}+\frac{\upsilon}{c_p}\left(2\left(\frac{\partial u}{\partial\eta}\right)^{2}-\frac{2}{3}\left(\frac{\partial u}{\partial\eta}\right)^{2}\right)\tag{16}$$

In spherical coordinates system (see, Hughes and Gaylord (1964)), (14) – (16) become

$$\frac{\partial u}{\partial t}=-\frac{1}{\rho}\frac{\partial p}{\partial r}+\upsilon\frac{\partial}{\partial r}\left(2\frac{\partial u}{\partial r}-\frac{2}{3}\frac{1}{r^{2}}\frac{\partial}{\partial r}\left(r^{2}u\right)\right)\tag{17}$$

$$\frac{\partial X_s}{\partial t} = \frac{D}{r^2}\frac{\partial}{\partial r}\left(r^2 \frac{\partial X_s}{\partial r}\right) \tag{18}$$

$$\frac{\partial T}{\partial t} = \frac{\lambda}{\rho c_p r^2}\frac{\partial}{\partial r}\left(r^2 \frac{\partial T}{\partial r}\right) + \frac{1000D}{M}\frac{\partial X_s}{\partial r}\frac{\partial T}{\partial r} + \frac{\upsilon}{c_p}\left(2\left(\frac{\partial u}{\partial r}\right)^2 + 4\left(\frac{u}{r}\right)^2 - \frac{2}{3}\left(\frac{\partial u}{\partial r} + \frac{2u}{r}\right)^2\right), \tag{19}$$

where u is the radial velocity.

The mole fraction of the solvent is directly deduced by the relation:

$$X_s = 1 - X_c \tag{20}$$

Darcy's law

$$u == -\frac{K}{\mu}\frac{\partial p}{\partial r} \tag{21}$$

To avoid potential convergence problems, the initial and boundary conditions is formulated as follows:

Initial condition:

At $t = 0$ and $\forall\ r$

$$u = U_{t0}, \quad T = \frac{1}{2}T_{s0}\left(1 + \tanh(\alpha(r - R))\right), \quad X_c = \frac{1}{2}X_{c0}\left(1 + \tanh(\alpha(r - R))\right)$$

(22)

Boundary conditions:

$$\left.\begin{array}{lll}
\left.\dfrac{\partial u}{\partial r}\right|_{r=0} = 0, & & \left.\dfrac{\partial u}{\partial r}\right|_{r=R} = q \\
\left.\dfrac{\partial X_s}{\partial r}\right|_{r=0} = 0, & D^1 \left.\dfrac{\partial X_s}{\partial r}\right|_{r=R} = k_m X_s\big|_{r=R} & \\
\left.\dfrac{\partial T}{\partial r}\right|_{r=0} = 0, & \lambda^1 \left.\dfrac{\partial T}{\partial r}\right|_{r=R} = hT\big|_{r=R}, & T_{c0} > T_{s0} \\
p\big|_{r=R} = p_{out} & &
\end{array}\right|$$

(23)

where X_c is the mole fraction of the carbon dioxide, X_s is the mole fraction of the solvent, D is the diffusion coefficient of the solvent in the carbon dioxide, ρ is the density of the binary mixture, λ is heat conductivity of the mixture, c_p is heat capacity of the mixture, K is the permeability, R is the droplet radius, T is the temperature of the mixture, M is the molecular weight, T_{c0} is the initial temperature of carbon dioxide, T_{s0} is the initial temperature of hydrocarbon, X_{c0} is the initial concentration of carbon dioxide, X_{s0} is the initial concentration of hydrocarbon, p is the pressure, u is the velocity of droplet, U_s is the surface velocity, μ is the dynamic viscosity, c_p is the constant pressure specific heat, r is the droplet radius, K is the permeability, D^1 is the effective diffusion coefficient, λ^1 is the effective heat conductivity, k_m is the convective mass transfer coefficient, h is the convective heat transfer coefficient, p_{out} is the outlet pressure, q is constant.

3. Method of Solution

3.2 Non-dimensionalisation

Dimensionless variables for space and time is been introduced as:

$$r' = \frac{r}{R}, \qquad t' = \frac{t}{t^*}, \qquad t^* = \frac{R}{U_s} \tag{24}$$

Dimensionless variables for velocity of droplet, mixture temperature, carbon dioxide mole fraction and hydrocarbon mole fraction is been introduced as follows:

$$\theta = \frac{T}{T_{s0}}, \qquad \phi = \frac{X_c}{X_{c0}}, \qquad \psi = \frac{X_h}{X_{h0}}, \qquad u' = \frac{u}{U_s}, \qquad p' = \frac{p}{\rho U_s^2} \tag{25}$$

where t^* is reference values for time.

Using (24) and (25), and after dropping the prime, equations (17) - (23) become

$$\frac{\partial u}{\partial t} = -\frac{\partial p}{\partial r} + \frac{4}{3}\frac{1}{R_e}\left(\frac{\partial^2 u}{\partial r^2} - \frac{1}{r}\left(\frac{\partial u}{\partial r} - \frac{u}{r}\right)\right) \tag{26}$$

$$\frac{\partial \phi}{\partial t} = \frac{1}{P_{em}}\frac{1}{r^2}\frac{\partial}{\partial r}\left(r^2 \frac{\partial \phi}{\partial r}\right) \tag{27}$$

$$\frac{\partial \theta}{\partial t} = \frac{1}{P_e}\frac{1}{r^2}\frac{\partial}{\partial r}\left(r^2 \frac{\partial \theta}{\partial r}\right) + \frac{\beta}{P_{em}}\frac{\partial \phi}{\partial r}\frac{\partial \theta}{\partial r} + \frac{4}{3} g \frac{E_c}{R_e}\left(\frac{\partial u}{\partial r} - \frac{u}{r}\right)^2 \tag{28}$$

$$\psi(r,t) = \sigma - \phi(r,t) \tag{29}$$

$$\frac{\partial p}{\partial r} = -\frac{1}{D_a R_e} u \tag{30}$$

$$\left.\begin{array}{lll} u(r,0) = 1, & u_r(0,t) = 0, & u_r(1,t) = \gamma \\ \phi(r,0) = \frac{1}{2}\left(1 + \tanh\left(\alpha'(r-1)\right)\right), & \phi_r(0,t) = 0, & \phi_r(1,t) = -Sh\phi(1,t) \\ \theta(r,0) = \frac{1}{2}\left(1 + \tanh\left(\alpha'(r-1)\right)\right), & \theta_r(0,t) = 0, & \theta_r(1,t) = -Nu\theta(1,t) \\ p_r(1,t) = \delta & & \end{array}\right\} \tag{31}$$

where

$R_e = \frac{RU_0}{\nu}$ is Reynolds number, $P_{em} = \frac{RU_0}{D}$ is Peclet mass number, $P_e = \frac{\rho c_p R U_0}{\lambda}$ Peclet energy number, $E_c = \frac{U_0^2}{c_p T_0}$ is Eckert number, $\sigma = \frac{1}{K_0}$, $\beta = \frac{1000 K_0}{M}$, $\alpha' = \alpha R$,

$D_a = \frac{K}{R^2}$ is Darcy number, $Sh = \frac{Rh_g}{D}$ is Sherwood number, $Nu = \frac{Rh}{\lambda}$ is Nusselt number,

$\gamma = \frac{Rq}{U_0}$, $A = \frac{P_m}{\rho U_0^2}$

3.4 Analytical Solution by Polynomial Approximation Method

Here, we assume polynomial solution of the form (see, Prakash and Mahmood (2015)):

$$\phi(r,t) = a_0(t) + a_1(t)r + a_2(t)r^2$$

(32)

$$u(r,t) = b_0(t) + b_1(t)r + b_2(t)r^2$$

(33)

$$\theta(r,t) = c_0(t) + c_1(t)r + c_2(t)r^2$$

(34)

Applying the boundary conditions as given in (31), we obtain

$$\begin{aligned} &a_1(t) = b_1(t) = c_1(t) = 0, \quad a_2(t) = -\frac{Sh}{2}\phi\big|_{r=1}, \quad b_2(t) = \frac{\gamma}{2}, \quad c_2(t) = -\frac{Nu}{2}\theta\big|_{r=1}, \\ &a_0(t) = \left(1 + \frac{Sh}{2}\right)\phi\big|_{r=1}, \quad b_0(t) = u\big|_{r=1} - \frac{\gamma}{2}, \quad c_0(t) = \left(1 + \frac{Nu}{2}\right)\theta\big|_{r=1} \end{aligned} \qquad (35)$$

Then, equation (32) – (33) become

$$\phi(r,t)=\left(1+\frac{Sh}{2}\right)\phi\big|_{r=1}-\frac{Sh}{2}\phi\big|_{r=1}r^2$$

(36)

$$u(r,t)=u\big|_{r=1}-\frac{\gamma}{2}+\frac{\gamma}{2}r^2$$

(37)

$$\theta(r,t)=\left(1+\frac{Nu}{2}\right)\theta\big|_{r=1}-\frac{Nu}{2}\theta\big|_{r=1}r^2$$

(38)

For long spherical shape (see, Keshavart and Taheri (2007)), we have

$$\bar{\phi}=3\int_0^1 r^2\phi dr$$

(39)

$$\bar{u}=3\int_0^1 r^2 u dr \tag{40}$$

$$\bar{\theta}=3\int_0^1 r^2\theta dr \tag{41}$$

where $\bar{\phi}$ is the average mole fraction, $\bar{u}$ is the average velocity, $\bar{\theta}$ is the average temperature.

Equations (39) – (41) give the relations

$$\bar{\phi}=\left(1+\frac{Sh}{2}\right)\phi\big|_{r=1}, \quad \bar{u}=u\big|_{r=1}-\frac{2\gamma}{5}, \quad \bar{\theta}=\left(1+\frac{Nu}{2}\right)\theta\big|_{r=1}$$

(42)

and

$$\frac{\partial}{\partial t}\bar{\phi}=\left(1+\frac{\delta h}{2}\right)\frac{\partial}{\partial t}\phi\Big|_{x=1},\quad \frac{\partial}{\partial t}\bar{u}=\frac{\partial}{\partial t}u\Big|_{x=1},\quad \frac{\partial}{\partial t}\bar{\theta}=\left(1+\frac{\delta\theta}{2}\right)\frac{\partial}{\partial t}\theta\Big|_{x=1}$$

(43)

Integrating (26) – (28) with respect to x, yield the following equations

$$\frac{\partial}{\partial t}\phi\Big|_{x=1}+\alpha\phi\big|_{x=1}=0$$

(44)

$$\frac{\partial}{\partial t}u\Big|_{x=1}-b\,u\big|_{x=1}=c$$

(45)

$$\frac{\partial}{\partial t}\theta\Big|_{x=1}+\left(A-Be^{-\alpha t}\right)\theta\big|_{x=1}=D\left(F-Ge^{bt}+E^{2}e^{2bt}\right) \qquad (46)$$

Solving (44) – (46) gives

$$\phi\big|_{x=1}=\frac{1}{2}e^{-\alpha t}$$

(47)

$$u\big|_{x=1}=\left(\left(\frac{c}{b}+1\right)e^{bt}-\frac{c}{b}\right)$$

(48)

$$\theta_{[illegible]} = [illegible]$$

(49)

Substituting equations (47) – (49) into equations (36) – (38) give

$$\phi(r,t) = \frac{1}{2}\left(1+\frac{Sh}{2}\right)e^{[illegible]} - \frac{Sh}{4}r^2 e^{[illegible]}$$

(50)

$$u(r,t) = \left(\left(\frac{c}{b}+1\right)e^{bt} - \frac{c}{b}\right) - \frac{\gamma}{2} + \frac{\gamma}{2}r^2$$

(51)

$$\theta(r,t) = \left(1+\frac{Nu}{2}\right)\theta_{[illegible]} - \frac{Nu}{2}\theta_{[illegible]}r^2$$

(52)

$$\psi(r,t)=\sigma-\frac{1}{2}\left(1+\frac{Sh}{2}\right)e^{-at}+\frac{Sh}{4}r^2e^{-at}$$

(53)

$$p(r,t)=\delta+\frac{1}{DaR_e}\left(\left(\left(\frac{c}{b}+1\right)e^{bt}-\frac{c}{b}\right)-\frac{\gamma}{3}\right)-\frac{1}{DaR_e}\left(\left(\left(\frac{c}{b}+1\right)e^{bt}-\frac{c}{b}\right)-\frac{\gamma}{2}+\frac{\gamma}{6}r^2\right)r$$

(54)

where

$$a=\frac{3Sh}{\left(1+\frac{Sh}{5}\right)P_{em}},\qquad b=\frac{1}{R_e}\left(4+\frac{1}{Da}\right),\qquad c=-\frac{1}{R_e}\left(\frac{4}{3}+\frac{1}{5Da}\right),$$

$$A=\frac{Nu}{\left(1+\frac{Nu}{5}\right)P_e},\qquad B=\frac{\beta NuSh}{10\left(1+\frac{Nu}{5}\right)P_{em}},\qquad D=\frac{4gEc}{3\left(1+\frac{Nu}{5}\right)R_e},$$

$$E=\left(\frac{c}{b}+1\right),\qquad \mathrm{F}=\left(\frac{4\gamma c}{3b}+\frac{4\gamma^2}{9}\right),\qquad \mathrm{G}=E\left(\frac{4\gamma}{3}+\frac{2c}{b}\right),$$

$$h(1)=e^{\frac{B}{a}}\left(\frac{1}{2}-\left(\begin{array}{l}FD\left(\frac{1}{A}\left(1-e^{-\frac{B}{a}}\right)-\frac{B}{A}\left(e^{\frac{B}{a}}-1\right)\right)-DG\left(\frac{1}{A+b}\left(1-e^{-\frac{B}{a}}\right)-\frac{B}{A+b}\left(e^{\frac{B}{a}}-1\right)\right)+\\ DE^2\left(\frac{1}{A+2b}\left(1-e^{-\frac{B}{a}}\right)-\frac{B}{A+2b}\left(e^{\frac{B}{a}}-1\right)\right)\end{array}\right)\right)$$

The computations were done on equations (50) – (54) using computer symbolic algebraic package MAPLE 16.

4. Results and Discussion

The transport and mixing processes are simulated analytically for a droplet of solvent (hydrocarbon) and a compressed antisolvent (carbon dioxide) in miscible conditions using polynomial approximation method. Analytical solutions given by equations (50) - (54) are computed using computer symbolic algebraic package MAPLE 16. The numerical results obtained from the method are shown in Figures 1 to 18. The temperature-time relationships is displayed in Figure 1. The carbon dioxide mole fraction-time relationships is displayed in Figure 2. The hydrocarbon mole fraction-time relationships is displayed in Figure 3. The velocity-time relationships is displayed in Figure 4. The pressure-time relationships is displayed in Figure 5. The relation between temperature and droplet radius is depicted in Figure 6. The relation between carbon dioxide mole fraction and droplet radius is depicted in Figure 7. The relation between hydrocarbon mole fraction and droplet radius is depicted in Figure 8. The relation between velocity of droplet and droplet radius is depicted in Figure 9. The relation between pressure and droplet radius is depicted in Figure 10. The relation among temperature, time and droplet radius are depicted in Figures 11 - 14. The relation among carbon dioxide mole fraction, time and droplet radius is depicted in Figures 15. The relation among hydrocarbon mole fraction, time and droplet radius is depicted in Figures 16. The relation among velocity of droplet, time and droplet radius is depicted in Figures 17. The relation among pressure, time and droplet radius is depicted in Figures 18.

Figure 1 depicts the graph of temperature $\theta(r,t)$ against time t for different values of droplet radius r. It is observed that the temperature of the mixture increases with time and it is higher at the centre of the droplet than at the end of the domain.

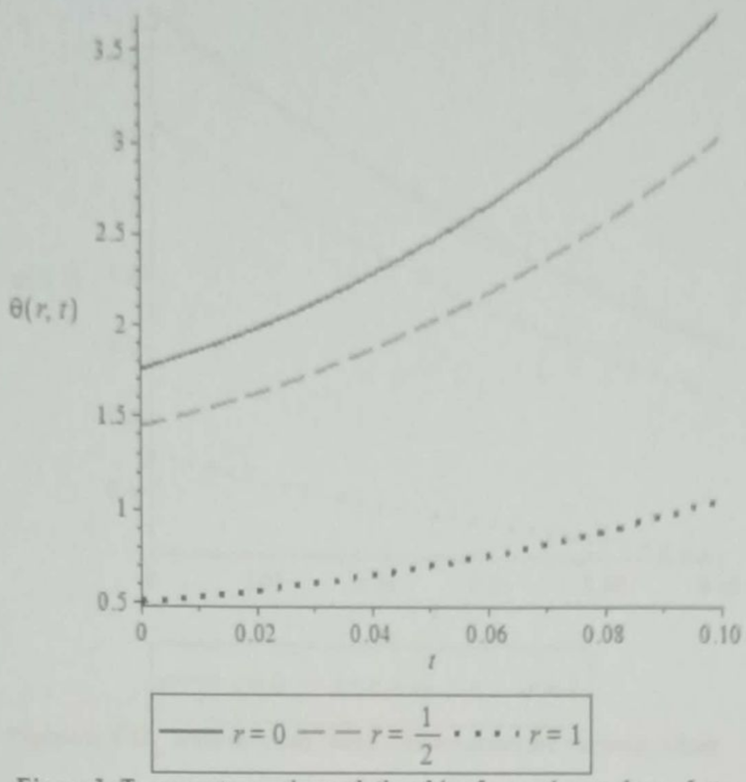

Figure 1: Temperature - time relationships for various values of r

Figure 2 shows the graph of carbon dioxide mole fraction $\phi(r,t)$ against time t for different values of droplet radius r. It is observed that the carbon dioxide mole fraction decreases with time and it is higher at the centre of the droplet than at the end of the domain.

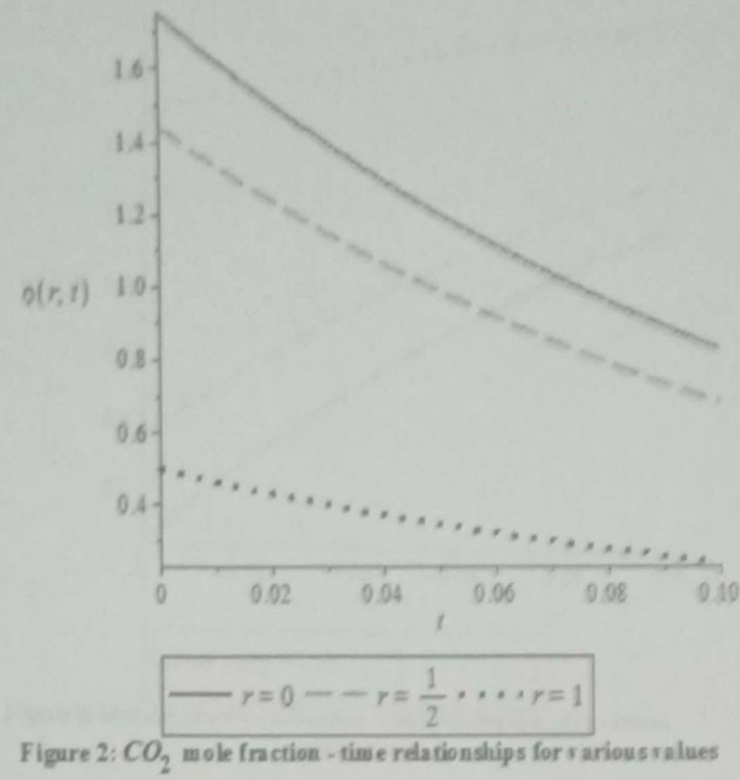

Figure 2: CO_2 mole fraction - time relationships for various values of r

Figure 3 displays the graph of hydrocarbon mole fraction $\psi(r,t)$ against time t for different values of droplet radius r. It is observed that the hydrocarbon mole fraction increases with time and it is higher at the end of the domain than at the centre of the droplet.

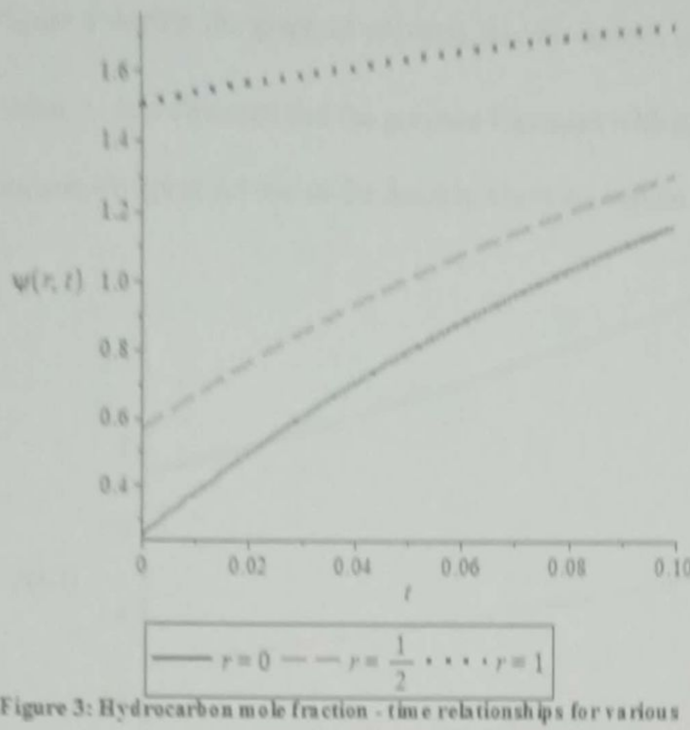

Figure 3: Hydrocarbon mole fraction - time relationships for various values of r

Figure 4 manifests the graph of velocity of droplet $u(r,t)$ against time t for different values of droplet radius r. It is observed that the velocity of droplet increases with time and it is higher at the end of the domain than at the centre of the droplet.

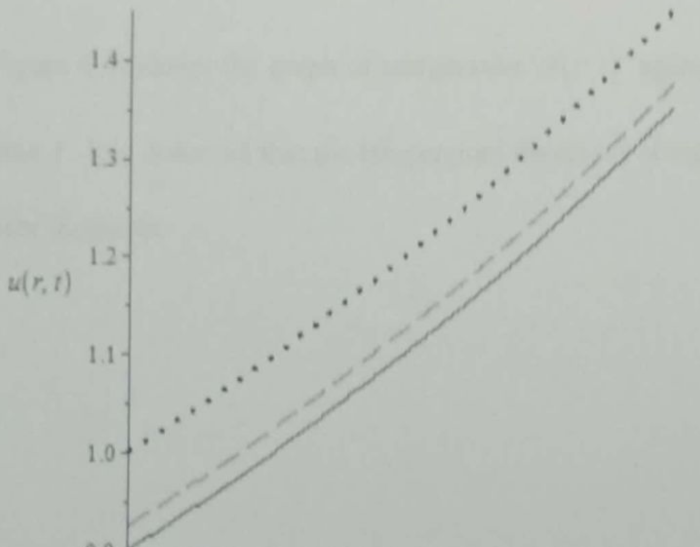

Figure 4: Velocity - time relationships for various values of r

Figure 5 depicts the graph of pressure $p(r,t)$ against time t for different values of droplet radius r. It is observed that the pressure increases with time and it is increases throughout the domain except at the end of the domain where it constant.

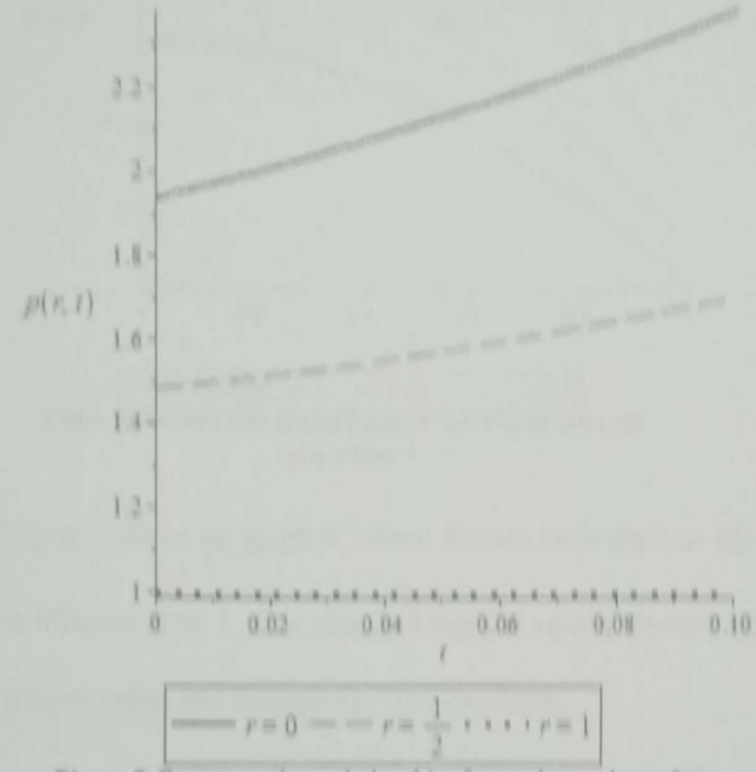

Figure 5: Pressure - time relationships for various values of r

Figure 6 discloses the graph of temperature $\theta(r,t)$ against the droplet radius r at different time t. It is observed that the temperature decreases along the droplet radius but increases as time increases.

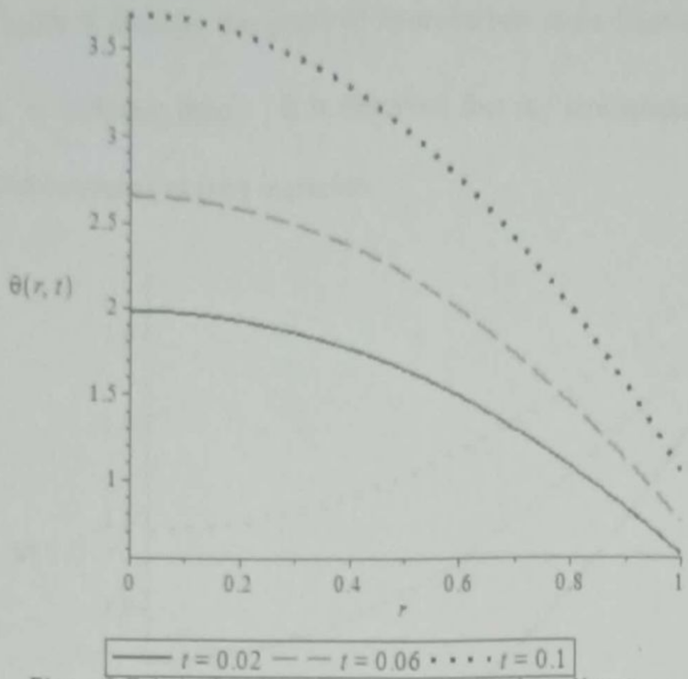

Figure 6: Relation between temperature and droplet radius at various time t

Figure 7 shows the graph of carbon dioxide mole fraction $\phi(r,t)$ against the droplet radius r at different time t. It is observed that the carbon dioxide mole fraction decreases along the droplet radius and decreases as time increases.

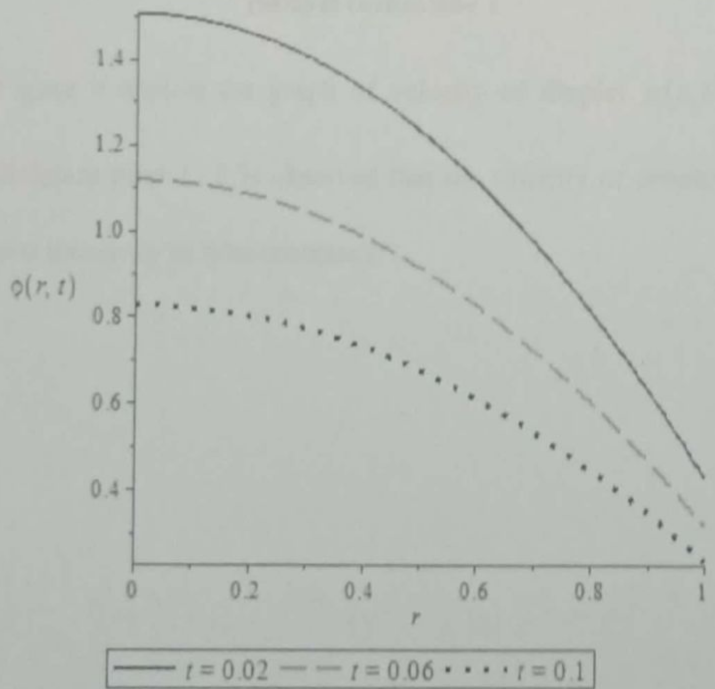

Figure 7: Relation between CO_2 mole fraction and droplet radius at various time t

Figure 8 displays the graph of hydrocarbon mole fraction $\psi(r,t)$ against the droplet radius r at different time t. It is observed that the temperature increases along the droplet radius and increases as time increases.

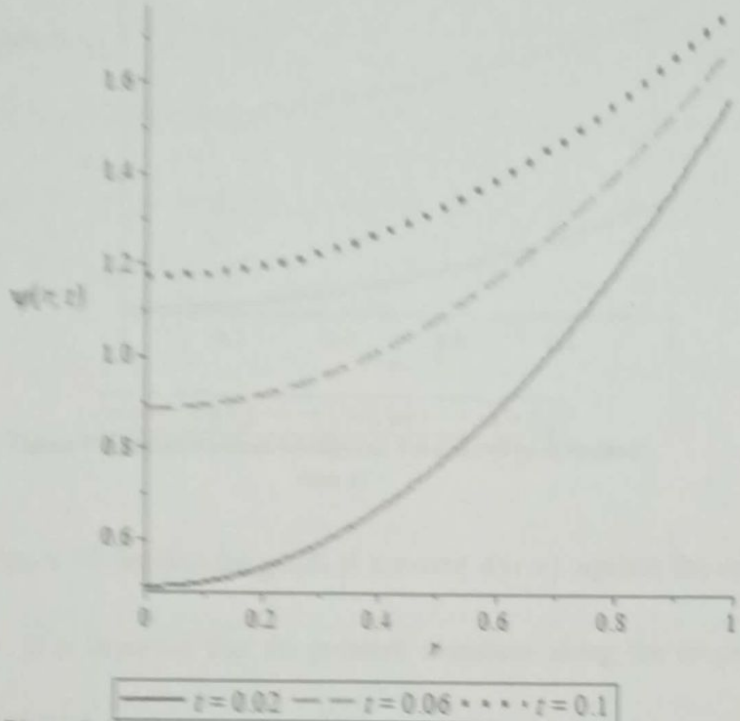

Figure 8: Relation between hydrocarbon mole fraction and droplet radius at various time t

Figure 9 depicts the graph of velocity of droplet $u(r,t)$ against the droplet radius r at different time t. It is observed that the velocity of droplet increases along the droplet radius and increases as time increases.

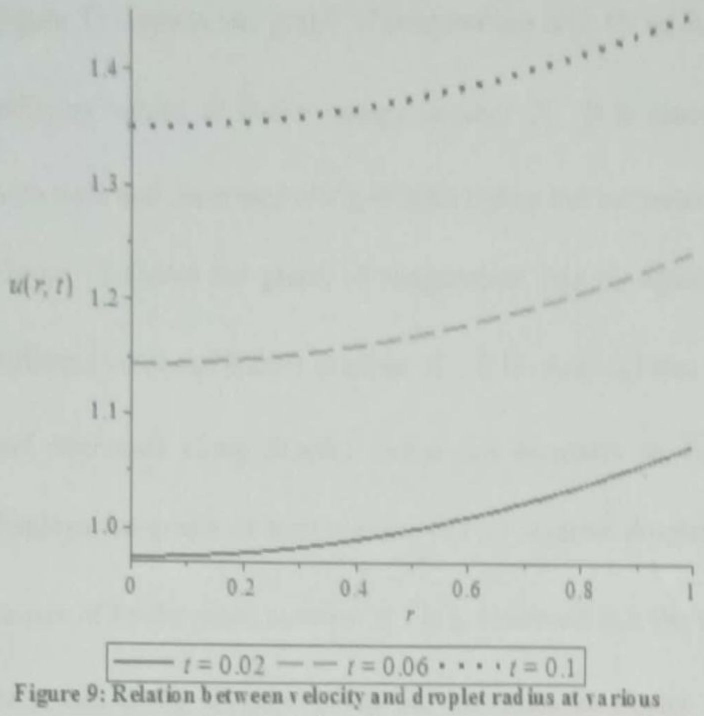

Figure 9: Relation between velocity and droplet radius at various time t

Figure 10 displays the graph of pressure $u(r,t)$ against the droplet radius r at different time t. It is observed that the pressure decreases along the droplet radius but increases as time increases.

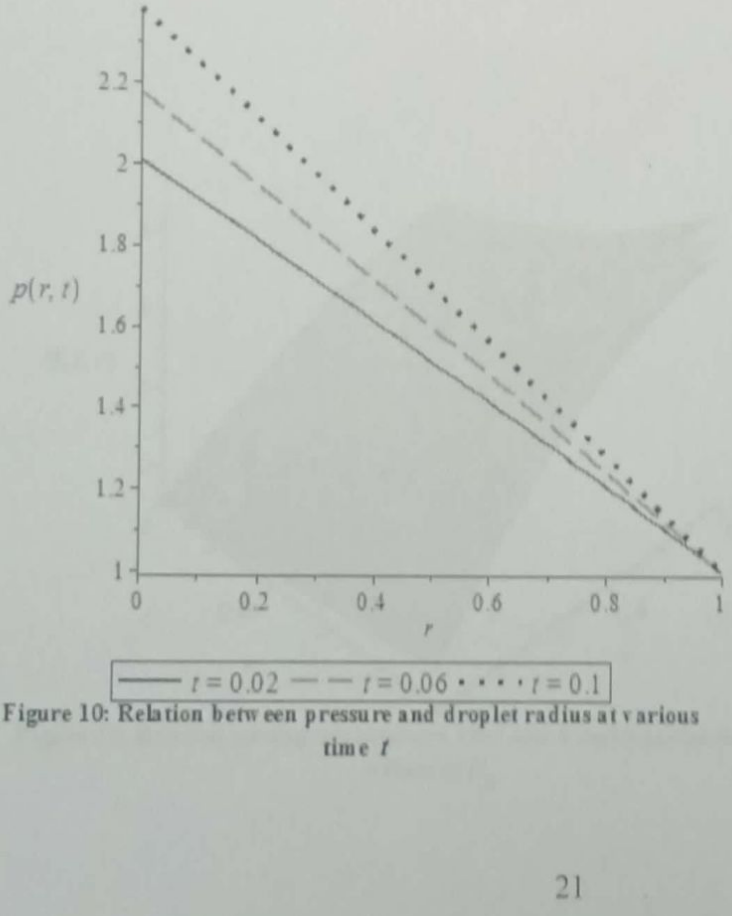

Figure 10: Relation between pressure and droplet radius at various time t

Figure 11 depicts the graph of temperature $\theta(r,t)$ against droplet radius r and time t for different values of Peclet energy number P_e. It is observed that the temperature increases with time and decreases along droplet radius but increases as Peclet energy number increases. Figure 12 shows the graph of temperature $\theta(r,t)$ against droplet radius r and time t for different values of Eckert number E_c. It is observed that the temperature increases with time and decreases along droplet radius but increases as Eckert number increases. Figure 13 displays the graph of temperature $\theta(r,t)$ against droplet radius r and time t for different values of Peclet mass number P_s. It is observed that the temperature increases with time and decreases along droplet radius but increases as Peclet mass number increases. Figure 14 displays the graph of temperature $\theta(r,t)$ against droplet radius r and time t for different values of Reynolds number R_e. It is observed that the temperature increases with time and decreases along droplet radius but decreases as Reynolds number increases.

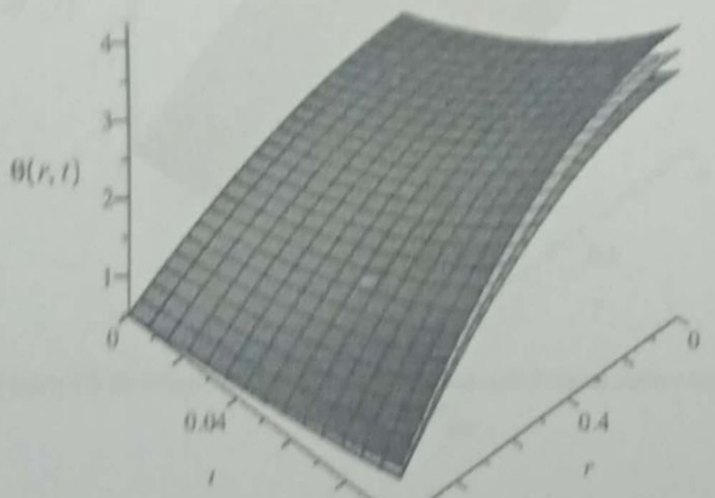

Figure 11: Relation among temperature, time and droplet radius for various values of P_e

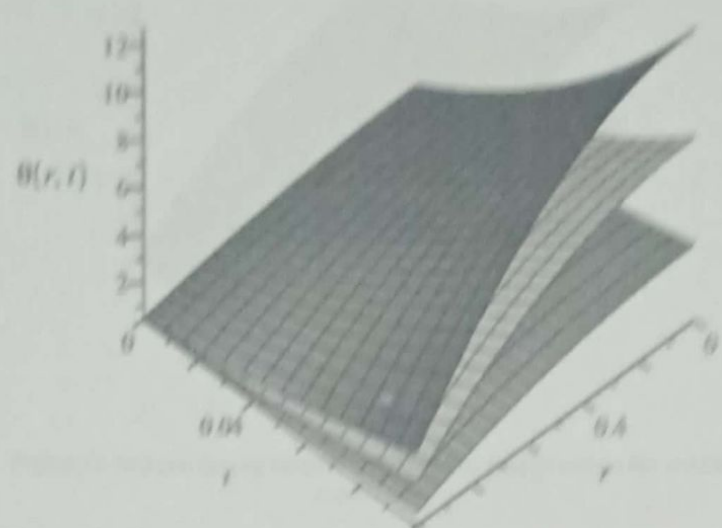

Figure 12: Relation among temperature, time and droplet radius for various values of E_t

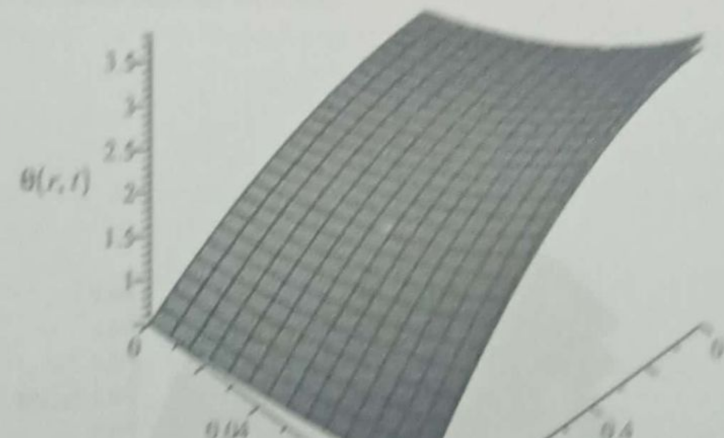

Figure 13: Relation among temperature, time and droplet radius for various values of P_{em}

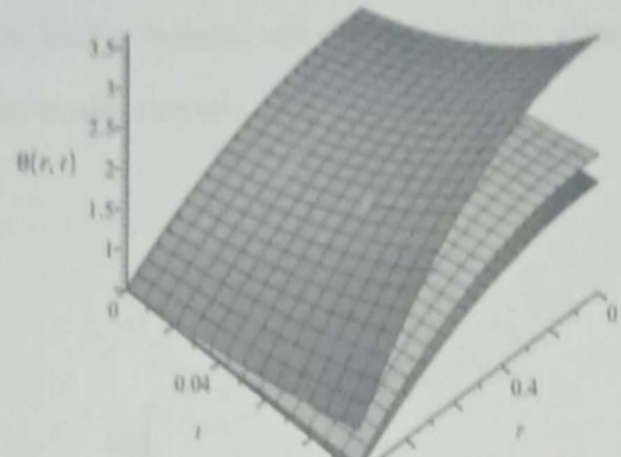

Figure 14: Relation among temperature, time and droplet radius for various values of R_e

Figure 15 shows the graph of carbon dioxide mole fraction $\phi(r,t)$ against droplet radius r and time t for different values of Peclet mass number P_e. It is observed that the carbon dioxide mole fraction decreases with time and decreases along droplet radius but increases as Peclet mass number increases.

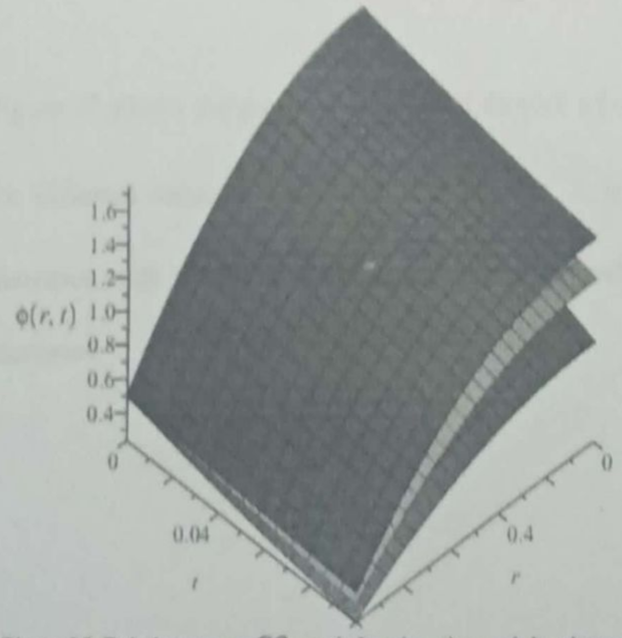

Figure 15: Relation among CO_2 mole fraction, time and droplet radius for various values of P_{em}

Figure 16 depicts the graph of hydrocarbon mole fraction $\psi(r,t)$ against droplet radius r and time t for different values of Peclet mass number P_{em}. It is observed that the hydrocarbon mole fraction increases with time and increases along droplet radius but decreases as Peclet mass number increases.

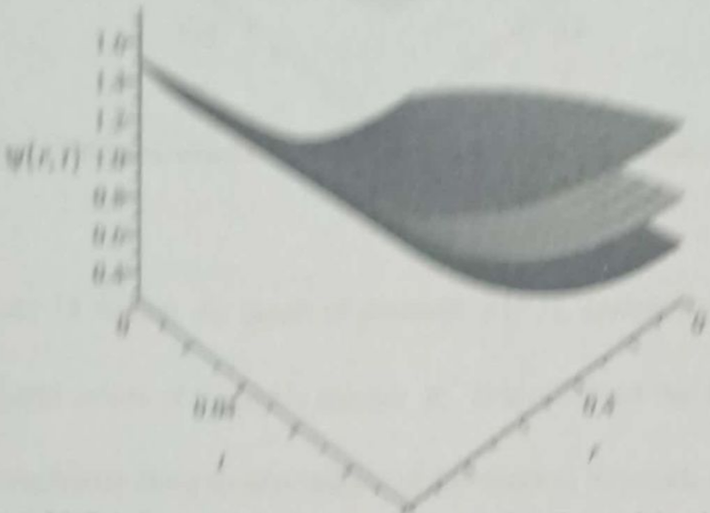

Figure 16: Relation among hydrocarbon mole fraction, time and droplet radius for various values of P_{em}

Figure 17 shows the graph of velocity of droplet $u(r,t)$ against droplet radius r and time t for different values of Reynolds number P_e. It is observed that the velocity of droplet increases with time and increases along droplet radius but decreases as Reynolds number increases.

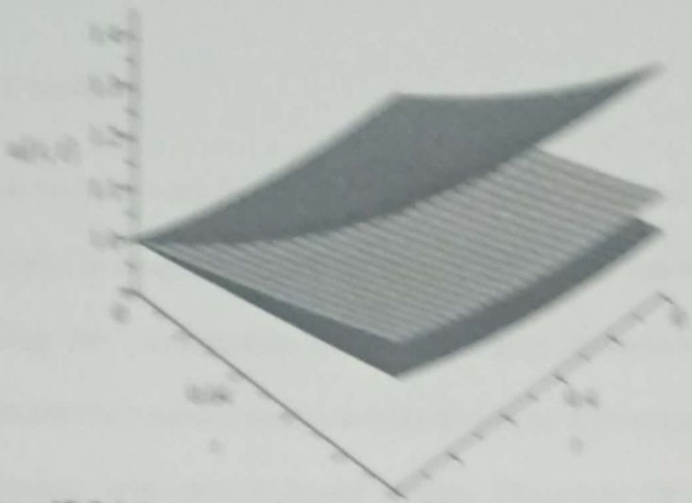

Figure 17: Relation among velocity, time and droplet radius for various values of R_e

Figure 18 depicts the graph of pressure $p(r,t)$ against droplet radius r and time t for different values of Reynolds number R_e. It is observed that the pressure increases with time and decreases along droplet radius but decreases as Reynolds number increases.

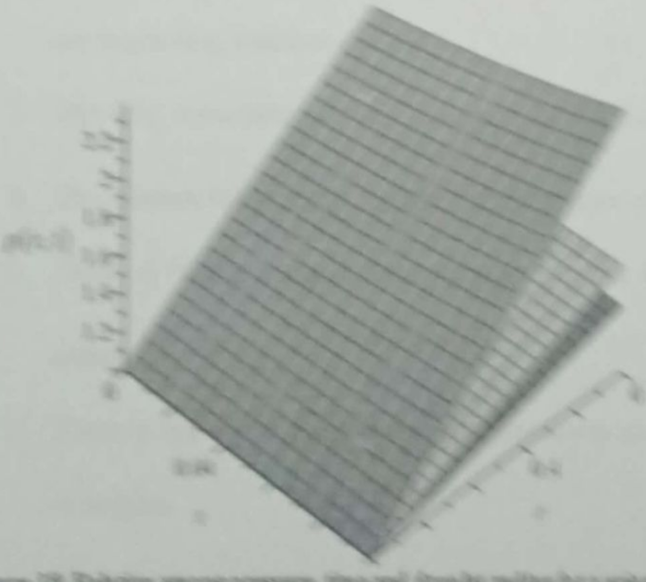

Figure 18: Relation among pressure, time and droplet radius for various values of R_e

It is worth pointing out that the effects observed in Figures 1 to 18, are important for designing and optimizing different CO_2 antisolvent processes for the formulation of small crystalline drug products.

5. Conclusion

This research work developed a model describing heat and mass transfer between a droplet of solvent (hydrocarbon) and a compressed antisolvent (carbon dioxide) in miscible conditions taking into consideration the viscous energy dissipation and transfer of heat and mass between the reservoir surface and the droplet by convection, in order to investigate the role of operating parameters on droplet lifetime. This model which relies on several assumptions is based on the conservation of total mass, chemical species, momentum and energy written in transient state mode of operation. The governing parameter of the problem are the Eckert number (E_c), Peclet energy number (P_e), Reynolds number (R_e), Peclet mass number (P_{em}), Darcy number (D_a), Nusselt number (Nu) and Sherwood number (Sh).The study revealed the following:

1. The mixture temperature, hydrocarbon concentration, pressure and velocity of droplet are increasing function of time.
2. The CO_2 concentration is a decreasing function of time.
3. The mixture temperature is higher at the centre of droplet than at the end of domain.
4. There is higher concentration of CO_2 at the centre of droplet than at the end of domain.
5. There is higher concentration of hydrocarbon at the end of domain than at the centre of droplet.
6. The velocity of droplet is higher at the end of domain than at the centre of droplet.

7. The pressure is higher at the end of domain than at the centre of droplet.

The results highlighted above showed that the particle formation in drug production could be controlled by the governing parameters involved. These results are useful in pharmaceutical industries for achieving very small drug particles of interest. The results of this study may be of importance to engineers and scholars attempting to develop programming standards and to researchers interested in the theoretical aspects of computer programming.

References

[1] Almeida R. A., Rezende R. V. P., Guirardello, R., Meier, H. F., Noriler D., Filho L. C. and Cabral V. F. (2015). Numerical Study of the Impact of the Solution Flow Rate in the Supercritical Antisolvent Process: a 3D Approach. *Chemical Engineering Transactions*, 43: 1633 – 1638.

[2] Budisa, N. and Schulze-Makuch, D. (2014). Supercritical Carbon Dioxide and Its Potential as a Life-Sustaining Solvent in a Planetary Environment. *Life* **2014**, 4, 331-340; doi:10.3390/life4030331.

[3] Chong, G. H., Spotar, S. Y. and Yunus, R. (2009). Numerical Modeling of Mass Transfer for Solvent-Carbon Dioxide System at Supercritical (Miscible) Conditions. *Journal of Applied Sciences*, 9 (17): 3055 – 3061.

[4] Hughes W. F. and Gaylord E. W. (1964). *Basic Equations of Engineering Science*. Schaum's Outline Series, McGraw-Hill Book Company, New York.

[5] Keshavarz P. and Taheri M. (2007). An improved lumped analysis for transient heat conduction by using the polynomial approximation method. *Heat Mass Transfer*, 43: 1151 – 1156.

[6] Kumar R., Mahalingam H and Tiwari K. (2012). Modeling of Droplet Composition in Supercritical Antisolvent Process: Part A. *International journal of Chemical Engineering and Application*, 3(6): 456 – 460.

[7] Olayiwola, R.O. (2015). Modeling and Simulation of Combustion Fronts in Porous Media. *Journal of Nigeria Mathematical Society*. **2** (1): 100 – 103.

[8] Padrela, L.; Rodrigues, M.A.; Velaga, S.P.; Matos, H.A.; Azevedo, E.G. (2009). Formation of indomethacin–saccharin cocrystals using supercritical fluid technology. *European Journal of Pharmaceutical Sciences*. **38** (1): 9 – 17.

doi:10.1016/j.ejps.2009.05.010. PMID 19477273

[9] Prakash A. and Mahmood S. (2013). Modified Lumped Model for Transient Heat Conduction in Spherical Shape. *American International Journal of Research in Science, Technology, Engineering & Mathematics*, 2(2): 155 – 159.

[10] Wu, G., Dabiri, S., Timko, M. T. and Ghoniem, A. F. (2012). Fractionation of multi-component hydrocarbon droplets in water at supercritical or near-critical conditions. *Journal of Supercritical Fluids*. 72: 150 – 160.

[11] Yash J. (2015). *Supercritical fluids and its applications*. A seminar report, Nirma University.